The synthesis of Au-NPs by ion implantation in the crystalline GaN and characterisation of their optical properties

Adéla Jagerová[1,2*], *Josef* Flaks[1], *Zdeněk* Sofer[3], *Marek* Vronka[4], *Alena* Michalcová[5] and *Anna* Macková[1,2]

[1]Nuclear Physics Institute of the Czech Academy of Sciences, 250 68 Řež, Czech Republic

[2]Department of Physics, Faculty of Science, J.E. Purkyne University, Pasteurova 3632/15, 400 96 Ústí nad Labem, Czech Republic

[3]Department of Inorganic Chemistry, University of Chemistry and Technology Prague, Technicka 5, 166 28 Prague 6, Czech Republic

[4]Institute of Physics of the Czech Academy of Sciences, Na Slovance 1999/2, 18221 Prague, Czech Republic

[5]Department of Metals and Corrosion Engineering, University of Chemistry and Technology, Technická 5, 166 28 Prague, Czech Republic

Abstract. Nanostructured surfaces with embedded noble metal nanoparticles is an attractive way for manipulation with the optical properties of wide bandgap semiconductors applied in optoelectronics, photocatalytic processes or for Surface-Enhanced Raman spectroscopy. Ion implantation offers an effective way for nanoparticle preparation without the use of additional chemicals that offers precise control of nanoparticle depth distribution. The aim of this study is a synthesis of the gold nanoparticles in GaN by implantation of 1.85 MeV Au ions with high fluences up to 7×10^{16} cm^{-2} and study of optical properties of Au implanted GaN. Implanted crystals were annealed at 800 °C in an ammonia atmosphere for 20 min to support Au nanoparticle creation and GaN recovery. The structure characterisation has been realized by Rutherford backscattering spectroscopy in channelling mode and it showed the formation of two separated disordered regions – the surface region and buried layer. The lower implantation fluences induce damage mainly in a buried layer; however, the increase of the Au-ion fluence leads to the increase of surface disorder as well. Further, the increase of the Au-ion fluence induces the Au dopant shift to the surface and multimodal Au-depth profiles. TEM analyses confirmed the formation of Au nanoparticles in the implanted samples after annealing with sizes up to 14 nm. The increase of light absorption and modification of GaN bandgap of the Au modified GaN was deduced from the change in optical transmission spectra between 370 – 1400 nm.

*Corresponding author: jagerova@ujf.cas.cz

1 Introduction

Nowadays, noble metal nanoparticles (NPs) such as Au NPs, Ag NPs, or Pt NPs are a perspective way for manipulation with properties of crystalline semiconductors. The modification of GaN or ZnO wurtzite semiconductors with noble metal NPs can enhance their photocatalytic properties and modify their optical properties. The interaction of Au NPs with GaN crystals can result in the enhancement of the intensity of near-band edge photoluminescence emission [1]. Further, the presence of a plasmonic layer of Au NPs can significantly affect the efficiency of GaN as a substrate for Surface-Enhanced Raman spectroscopy (SERS) application, increase the intensity of SERS peaks and improve detection limits e.g. for cancer detection via miRNA solution [2,3].

The implantation of energetic metal ions with high fluence leads to the aggregation of dopant and can be applied as an interesting method for the preparation of metal-based NPs. Generally, this process involves several stages, depending on the implantation fluence, and it includes saturation of implanted ion concentration, further a start of dopant aggregation, nanoparticle growth, and formation of large particles at the expense of smaller ones known as an Ostwald ripening or coalescence of created nanoparticles into the compact layer. It is necessary to understand this process to maintain particle synthesis in the nanoscale dimension [4].

The ion beam method can be used for NPs preparation in selected depth, without the use of chemical additives [5]. However, it leads to high radiation damage, especially in the case of crystalline materials leading to the degradation of crystal properties. Therefore, there is still a need to study the implantation process with subsequent annealing for NPs preparation in connection to the optical response of prepared nanostructures.

The implantation of iron Fe^{+} with energy 200 keV into the epitaxial layers of wurtzite gallium nitride (GaN) [6] leads to the formation of small clusters with a size 8 nm. The optical properties of lithium niobate ($LiNbO_3$) [7] were tailored by the Ag NPs prepared by implantation of Ag ions with energy 200 keV and fluences in the range of $5x10^{16}$ - $1x10^{17}$ cm^{-2}. Similar fluences were used also for the preparation of Cu NPs with diameter size 10 nm in single-crystalline silicon Si [8].

In this work, we implanted *c-plane* GaN single crystal substrates by energetic Au ions with a wide range of ion fluences to see particular stages of ion implantation induced NPs formation and their effect on the optical response of GaN crystal.

2 Experiment

The single crystal *c-plane* (0001) GaN substrates were implanted with 1.85 MeV Au ions with constant current density 270 nA/cm^2 at incidence 7° with high ion fluences in the range of 1.5×10^{16} cm^{-2} up to 7×10^{16} cm^{-2}, where the aggregation of Au ions and creation of Au NPs is expected. The projected range R_P of 1.85 MeV Au ions was estimated by the SRIM program as 229 nm with a standard deviation of ΔR_P = 64 nm. The substrate holder was not directly cooled during the implantation experiment and substrate temperature increases up to 130 °C, as it was measured immediately after the implantation experiment. The 1.85 MeV Au ions were produced by the Tandetron accelerator in the Nuclear Physics Institute of CAS in Řež (Czech Republic). The implanted GaN substrates were annealed at 800 °C for 20 minutes in an ammonia atmosphere to support nucleation and growth of Au NPs. The structural characterisation of the implanted, as well as annealed GaN samples,

were carried out by Rutherford backscattering spectroscopy (RBS-C) with a 2.8 MeV He^+ ion beam produced by Tandetron accelerator in Řež as well.

The visualization of prepared Au NPs was carried out on the implanted samples after annealling by transmission electron microscopy (TEM) measurement. Samples for transmission electron microscopy (TEM) were prepared as lamellas by focused ion beam SEM technique. HTEM (High-resolution transmission electron microscopy) and STEM (scanning transmission electron microscopy) observations were carried out by Fei Tecnai F20 field emission gun transmission electron microscope operated at 200 kV equipped with an EDS detector which confirmed the presence of Au NPs. For STEM, Z-contrast imaging was performed using a high angle annular dark field (STEM–HAADF) detector.

The optical response of the implanted GaN substrates before and after annealing was analysed by measurement of transmission spectra in the UV-Vis region. Transmission spectra were measured perpendicularly to the GaN surface with UVISEL plus Spectroscopic Ellipsometer from Horiba (France) in the spectral range 190-1400 nm with a step 5nm.

3 Results and discussion

As it is seen in RBS-C spectra presented in
Fig. 1a, the implantation of Au ions leads to the increase of yield of backscattered ions from Ga (channels up to 540) even for the lowest Au-ion fluence 1.5×10^{16} cm^{-2}. The backscattered ion yield in RBS-C spectra is connected to the growth of Ga-sublattice disorder and the displacement of Ga atoms from their original positions. The ion implantation of GaN crystals forms two damage regions. Firstly, the buried layer corresponds to the depth of implanted ions (channels 410 – 460). An increase in implantation fluence leads to the saturation of damage in the buried layer. The damage level characterised by the normalized yield χ_{norm} achieved more than 71 % for the sample implanted with fluence 1.5×10^{16} cm^{-2}, for the higher fluences saturates at around 80 %. Defect migration towards the surface is forming a second surface damage region (channels 460 – 525). In this region, χ_{norm} gradually increases from 56 % for the lowest implantation fluence up to 95 % for the fluence 7×10^{16} cm^{-2}. For the highest implantation fluence 7×10^{16} cm^{-2}, the yield of backscattered ions in the surface damage region reaches a level of random spectra indicating nearly complete amorphisation of the surface or creation of randomly oriented nanocrystals and voids [9,10].

The low temperature (200 K) 2 MeV Au GaN implantation, with the high implantation fluences leads to the significant change in crystal damage and to the creation of surface and buried amorphous layers for fluences above 1.4×10^{15} cm^{-2} as is presented in [11]. In our experiment, only the surface amorphous region was observed. During the ion implantation at room temperature, GaN exhibits strong dynamic annealing which prevents bulk crystals to reach complete amorphisation in a depth. Instead of this, GaN amorphisation proceeds layer-by-layer from the GaN surface [12]. Further, the high ion fluence bombardment tends to induce preferential nitrogen loss from the GaN surface [12] as it was also observed in this experiment by an increase of Ga amount in the surface layer in a random spectrum of the sample implanted with the highest fluence 7×10^{16} cm^{-2} (see **Fig. 1a**). The post implantation annealing in the ammonia atmosphere leads to crystal recovery and reorganization mainly in the surface region, as is seen in **Fig. 1b**. The annealing in an atmosphere with an excess of nitrogen can protect the GaN surface against disintegration and compensate for nitrogen loss by the creation of new Ga-N bonds during high-temperature annealing [13].

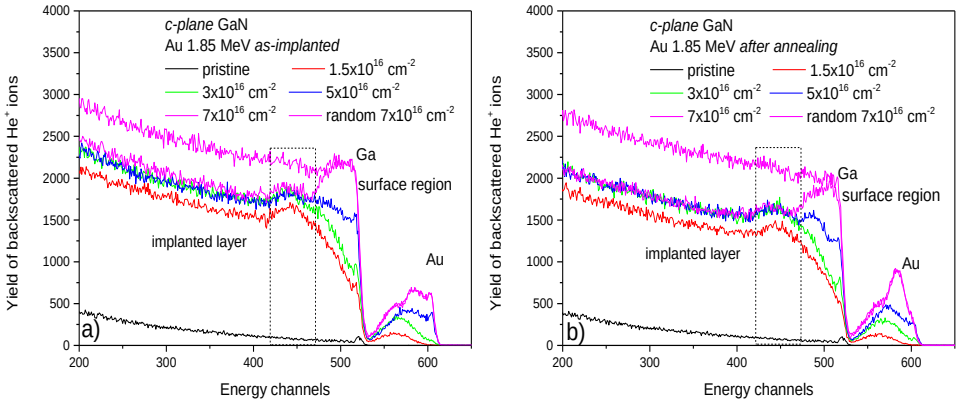

Fig. 1. RBS-C spectra of GaN pristine as well as the samples implanted with Au ions with energy 1.85 MeV in a), and corresponding samples after 20 minutes of annealing at 800 °C in ammonia atmosphere in b)

RBS-C analysis serves also for the Au-ion depth profiling which was evaluated from random spectra. In **Fig. 2a** we can see a comparison of SRIM calculated Au-depth distribution to the experimentally determined Au-depth profiles after the ion implantation. For the lower implantation fluences, up to 3×10^{16} cm^{-2}, the Au depth distribution has a Gaussian profile and agrees with SRIM prediction. With an increase of ion implantation fluence, the Au starts to migrate towards the GaN surface and create multimodal depth profiles with additional concentration maxima. It was observed that Au ions diffuse to the GaN surface region where the high disorder nearly amorphous structure is present [11,14]. Annealing induces reorganization of Au depth profiles for the samples implanted with fluence 5×10^{16} cm^{-2} and higher, as is seen in **Fig. 2b**. The most significant change of Au depth distribution is observed for the sample implanted with the highest Au-ion fluence, where a sharp Au-concentration maximum appeared in the depth of 125 nm. The integrated Au-content stays constant before and after annealing.

It was shown that thermal or laser annealing can significantly affect the formation process of metal NPs. The annealing support movement of implanted Au ions towards the region with extended defects serving as trapping sites for implanted ions [15]. This leads to the dopant depth redistribution and enhancement of Ostwald ripening and coalescence of NPs [15]. Such phenomenon is suggested to take place also in our case, where probably Au-redistribution and NPs coalescence take a place.

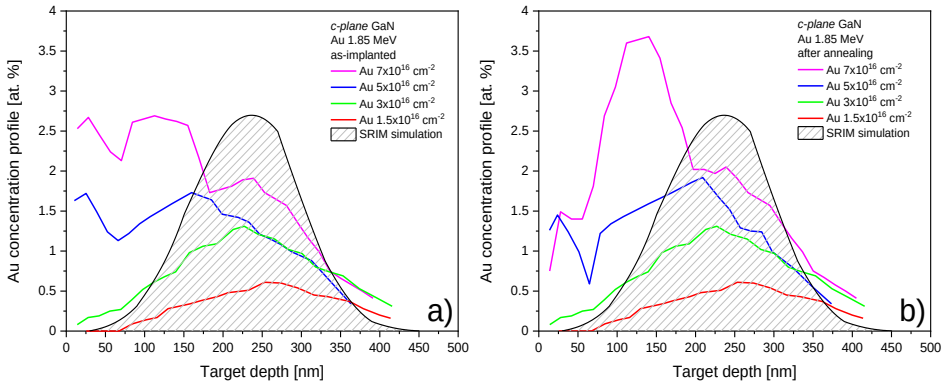

Fig. 2. – The comparison of SRIM calculated Au-depth distribution corresponding to the fluence 5×10^{16} cm^{-2} of 1.85 MeV Au ions with the experimentally determined Au-concentration depth profiles in a) and after the subsequent annealing in b)

TEM analysis was performed on the implanted GaN samples after the thermal annealing. Implanted Au ions tend to aggregate and create small clusters with sizes up to several nm up to the depth of almost 300 nm, see cross-sectional STEM image in **Fig. 3a**. These small Au NPs have a diameter in a range of 4 - 15 nm. The STEM image of GaN implanted with ion fluence 7×10^{16} cm^{-2} presented in **Fig. 3a** is superimposed with Au ion depth distribution obtained from RBS-C. The biggest Au NPs are distributed in depth from 70 nm up to 180 nm corresponding to the maximum of Au distribution determined by RBS-C. Above this depth, the amount of Au NPs decreases and large Au agglomerates are presented up to 300 nm. The dark spots belong to extended defects and voids in the highly damage region of GaN implanted with 2 MeV Au ions observed in [11]. The structure and lattice spacing in Au NPs were determined by HRTEM analysis with Fast Fourier Transformation (FFT); see **Fig. 3b** and **Figure 3c**. Prepared Au NPs exhibits a face-centred cubic (*fcc*) structure with d-spacing of 0.38 nm. The *fcc* structure is typical for pure gold and it was already observed for Au NPs prepared by the ion implantation of Au ions to the silica glass [16] as well as for Au NPs colloid solution prepared by standard chemical preparation procedure from Au salts [17]. In our experiment, the d-spacing of prepared Au NPs is lower than the d-spacing of pure Au 0.41 nm [17,18] which may be attributed to internal strain.

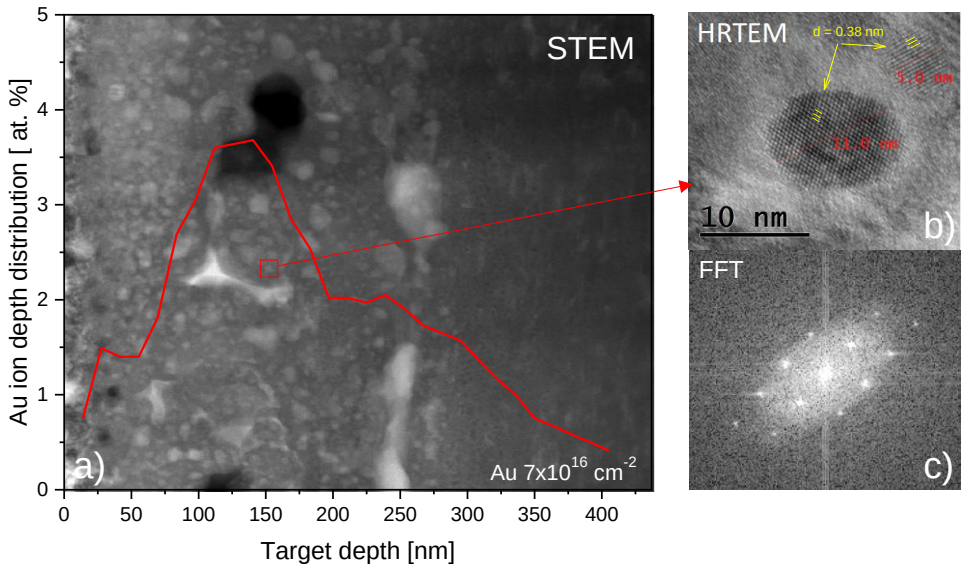

Fig. 3. Cross-sectional STEM image of GaN sample implanted with the Au-ion fluence 7×10^{16} cm^{-2} after annealing in a) and HRTEM analysis of Au NPs with diffractogram in b) and corresponding FFT pattern of the bigger Au NPs.

The optical response of the Au-ion implanted, as well as subsequently annealed, GaN samples was characterized by optical transmission spectra in a range 190-1400 nm presented in **Fig.4**. The GaN is transparent for photons with energy lower than GaN bandgap energy (3.4 eV [19]). Therefore, the pristine GaN exhibits transmission above 60 % for light with a wavelength higher than 370 nm. The light with a wavelength lower than 370 nm is absorbed in GaN. Optical transmission in the wavelength range 370 – 1400 nm is influenced by the Au-ion implantation, generally, the optical transmission decreases with the growing Au-ion implantation fluence. This fact is connected to the higher crystal disorder. For the highest Au-ion fluence 7×10^{16} cm^{-2}, the optical transmission is strongly suppressed in the wavelength above 370 nm and the sample appears nearly opaque. Additionally, the transmission edge is shifted towards higher wavelengths. This indicates the lowering of bandgap energy with implantation fluence, as is presented in **Fig. 4a**. The modification and lowering of bandgap energy can be attributed to the strain caused by incorporated Au ions and growing structure disorder as it was already observed for a similar structure of ZnO modified with Au NPs [20].

The post implantation annealing leads to the crystal recovery as it was observed by RBS-C and it results in an increase of the optical transmission in the wavelength range of 370 - 1400, see **Fig. 4b.** The recovery effect is seen especially for the lower implantation fluences up to 3×10^{16} cm^{-2}, where the transmittance spectrum reaches the level of the pristine GaN above the wavelength of 800 nm. The shift of the transmission edge towards higher wavelengths indicates a decrease of bandgap energy due to crystal recovery and the lowering of lattice strain after the annealing. Nevertheless, the position of the transmission edge still indicates some persisting damage even after the annealing. Further, the Au NPs are characterised by increased absorption due to the Surface plasmon resonance (SPR) leading to the creation of a dip between 500 – 600 nm in transmission spectra [20], which is not observed in our experiment. It can be assumed that Au NPs are located in a depth of GaN and their volume fraction in GaN samples is too low to allow propagation of SPR response in the transmission spectra similarly as it was evidenced for Cu NPs synthesised by ion implantation in ITO layers in [21].

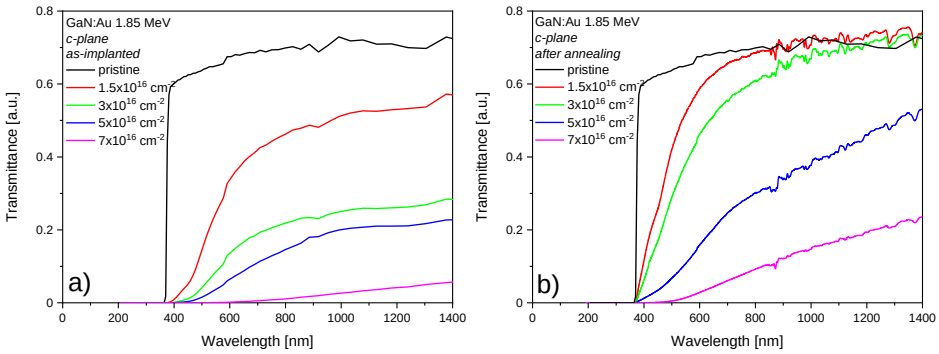

Fig. 4. Optical transmittance spectra of the pristine and Au-ion implanted GaN in a) and the subsequently annealed GaN samples in b)

4 Conclusion

The ion implantation of 1.85 MeV Au ions into the *c-plane* GaN crystals followed by thermal annealing at 800°C in an amonia atmosphere has been applied for the preparation of Au NPs to modify GaN optical properties. The Au-ion implantation with high fluences leads to the Ga-sublattice disorder enhancement in the implanted layer as well as to the additional disordered layer created at the surface with thickness about 150 nm for the Au-ion fluence above 5×10^{16} cm^{-2}. Above this Au-ion fluence, the creation of the Au-multimodal depth profiles was observed. The annealing induced partial crystal recovery in the implanted layer and a significant improvement of the surface layer ordering as it was deduced from RBS-C analysis. Simultaneously, the implanted Au depth profiles exhibited a sharp Au-concentration maximum which may be related to the Oswald ripening and growth of Au NPs. The TEM analysis confirmed the formation of small Au NPs of the sizes 1 – 15 nm in the implanted GaN after annealing. TEM showed Au NPs exhibiting cubic *fcc* structure with d-spacing of 0.38 nm. Au-ion implantation leads to the suppression of the optical transmission above 370 nm with a growing Au-ion implantation fluence. This effect is partially recovered after the annealing and mainly for the Au-ion fluences below 5×10^{16} cm^{-2}.

The research has been carried out at the CANAM (Centre of Accelerators and Nuclear Analytical Methods) infrastructure LM 2015056. This publication has been supported by OP RDE, MEYS, the Czech Republic, under the project CANAM OP, CZ.02.1.01/0.0/0.0/16_013/0001812 and promoted by the University of J.E. Purkyne project UJEP-SGS-2021-53-002-2

References

1. I.-H. Lee, L.-W. Jang and A. Y. Polyakov, *Nano Energy*, **13**, 140–173 (2015)
2. Y. Han, L. Qiang, Y. Gao, J. Gao, Q. He, H. Liu, L. Han and Y. Zhang, *Applied Surface Science*, **541**, 148456 (2021)
3. I. Dzięcielewski, J. Smalc-Koziorowska, M. Bańkowska, T. Sochacki, A. Khachapuridze and J. Weyher, *Applied Surface Science*, **378**, 30–36 (2016)
4. F. Chen, H. Amekura and Y. Jia, in *Ion Irradiation of Dielectrics for Photonic Applications*, Springer Singapore, Singapore, vol. 231, pp. 61–107 (2020)

5. M. E. Koleva, N. N. Nedyalkov, Ru. Nikov, Ro. Nikov, G. Atanasova, D. Karashanova, V. I. Nuzhdin, V. F. Valeev, A. M. Rogov and A. L. Stepanov, *Applied Surface Science*, **508**, 145227 (2020)
6. G. Talut, H. Reuther, A. Mücklich, F. Eichhorn and K. Potzger, *Appl. Phys. Lett.*, **89**, 161909 (2006)
7. C. Pang, R. Li, Y. Zhang, Z. Li, N. Dong, L. Wu, H. Yu, J. Wang, F. Ren and F. Chen, *Opt. Express*, **26**, 31276 (2018)
8. A. I. Gumarov, A. M. Rogov and A. L. Stepanov, *Composites Communications*, **21**, 100415 (2020)
9. F. Gloux, T. Wojtowicz, P. Ruterana, K. Lorenz and E. Alves, *Journal of Applied Physics*, **100**, 073520 (2006)
10. M. Ishimaru, Y. Zhang and W. J. Weber, *Journal of Applied Physics*, **106**, 053513 (2009)
11. Y. Zhang, M. Ishimaru, J. Jagielski, W. Zhang, Z. Zhu, L. V. Saraf, W. Jiang, L. Thome and W. J. Weber, *J. Phys. D: Appl. Phys.*, **43**, 085303 (2010)
12. S. O. Kucheyev, J. S. Williams and S. J. Pearton, *Materials Science and Engineering: R: Reports*, **33**, 51–108 (2001)
13. C. Ronning, *Physics Reports*, **351**, 349–385 (2001)
14. A. Macková, P. Malinsky´, A. Jágerová, Z. Sofer, D. Sedmidubský, K. Klímová, R. Böttger and S. Akhmadaliev, *Surf Interface Anal*, **50**, 1099–1105 (2018)
15. M. Steinert, W. Wesch, A. Undisz, M. Rettenmayr, W. C. Nunes, R. P. Borges, M. Godinho, R. M. Rubinger, M. C. Carmo and N. A. Sobolev, *J. Phys. D: Appl. Phys.*, **42**, 035406 (2009)
16. H. G. Silva-Pereyra, J. Arenas-Alatorre, L. Rodriguez-Fernández, A. Crespo-Sosa, J. C. Cheang-Wong, J. A. Reyes-Esqueda and A. Oliver, *J Nanopart Res*, **12**, 1787–1795 (2010)
17. D. Lomelí-Marroquín, D. Medina Cruz, A. Nieto-Argüello, A. Vernet Crua, J. Chen, A. Torres-Castro, T. J. Webster and J. L. Cholula-Díaz, *IJN*, **14**, 2171–2190 (2019)
18. O. Peña, U. Pal, L. Rodríguez-Fernández, H. G. Silva-Pereyra, V. Rodríguez-Iglesias, J. C. Cheang-Wong, J. Arenas-Alatorre and A. Oliver, *J. Phys. Chem. C*, **113**, 2296–2300 (2009)
19. Y.-T. Chen, C.-Y. Yang, P.-C. Chen, J.-K. Sheu and K.-H. Lin, *Sci Rep*, **7**, 5788 (2017)
20. R. Sreeja Sreedharan, V. S. Kavitha, S. Suresh, R. Reshmi Krishnan, R. Jolly Bose and V. P. Mahadevan Pillai, *Appl. Phys. A*, **124**, 815 (2018)
21. A. I. Ryasnyansky, B. Palpant, S. Debrus, R. I. Khaibullin and A. L. Stepanov, *J. Opt. Soc. Am. B*, **23**, 1348 (2006)